

Full oxide heterostructure combining a high- T_C diluted ferromagnet with a high-mobility conductor

G. Herranz,¹ M. Basletic,² M. Bibes,³ R. Ranchal,⁴ A. Hamzic,² E. Tafr, ²
K. Bouzehouane,¹ E. Jacquet,¹ J. P. Contour,¹ A. Barthélémy,¹ and A. Fert¹

¹*Unité Mixte de Physique CNRS / Thales, Route Départementale 128, 91767 Palaiseau, France**

²*Dep. of Physics, Fac. of Science, HR-10002 Zagreb, Croatia*

³*Institut d'Électronique Fondamentale, Univ. Paris-Sud, 91405 Orsay, France*

⁴*Depto. Física de Materiales (UCM), Ciudad Universitaria s/n Madrid 28040, Spain*

(Dated: June 21, 2018)

We report on the growth of heterostructures composed of layers of the high-Curie temperature ferromagnet Co-doped (La,Sr)TiO₃ (Co-LSTO) with high-mobility SrTiO₃ (STO) substrates processed at low oxygen pressure. While perpendicular spin-dependent transport measurements in STO//Co-LSTO/LAO/Co tunnel junctions demonstrate the existence of a large spin polarization in Co-LSTO, planar magnetotransport experiments on STO//Co-LSTO samples evidence electronic mobilities as high as $\sim 10^4$ cm²/Vs at T = 10 K. At high enough applied fields and low enough temperatures ($\mu H \geq 6$ Teslas, T ≤ 4 K) Shubnikov-de Haas oscillations are also observed. We present an extensive analysis of these quantum oscillations and relate them with the electronic properties of STO, for which we find large scattering rates up to $\approx 10^{-11}$ s. Thus, this work opens up the possibility to inject a spin-polarized current from a high-Curie temperature diluted oxide into an isostructural system with high-mobility and a large spin diffusion length.

PACS numbers: 72.25.Hg, 73.50.Fq, 75.50.Pp

I. INTRODUCTION

The early years of spintronics have focused on the giant magnetoresistance (GMR) of magnetic metallic multilayers¹, and the tunnel magnetoresistance of magnetic tunnel junctions combining metallic ferromagnets and insulating barriers². Both have led to interesting devices such as magnetoresistive read heads, sensors and an incoming new generation of non volatile magnetic random access memories (MRAMs).

Further developments in spintronics³ now aim at combining ferromagnets with semiconductors in order to, for instance, modulate spin-polarized transport by a gate voltage. This functionality opens exciting perspectives, but is prohibited in fully metallic structures because of the large carrier density ($n \approx 10^{22}$ cm⁻³). Unfortunately, at the interface between a ferromagnetic metal (FM) and a semiconductor (SC) spin-flip events (inversely proportional to the resistivity ρ times the spin diffusion length l_{sf}) lead to an almost complete loss of the spin polarization inside the metallic ferromagnet due to the difference in the resistivities between the two materials^{4,5}. Such a loss is not observed in metallic multilayers such as Co/Cu, due to the similarity of their $\rho \times l_{sf}$ products, and an efficient spin injection can occur in Cu. It has been suggested that introducing a spin-dependent resistance at the FM/SC interface can solve this problem of "conductivity mismatch"^{5,6}. Yet, one of the best solutions would be to realize heterostructures combining highly spin-polarized ferromagnets and non-magnetic materials with similar resistivities, to enable efficient spin injection (in the ohmic regime), and low carrier density, to enable

gate voltage effects.

Most efforts in this direction have focused on semiconductor structures using II-VI or III-V diluted magnetic semiconductors (BeZnMnSe⁷ or (Ga,Mn)As⁸) as spin-polarized injectors. Since the Curie temperature (T_C) of (Ga,Mn)As is lower than about 170K⁹, such devices are limited to low-temperature operation.

Oxide materials have not been considered so far but should be interesting candidates since high- T_C ferromagnetism has been reported in diluted magnetic oxide systems (DMOS) like Co-doped TiO₂¹⁰ and ZnO¹¹ for instance. In addition, high- T_C ferromagnetism was recently found in La- and Co-doped SrTiO₃ thin films^{12,13}. In this paper we present results on structures combining (La, Sr)Ti_{1-x}Co_xO₃ (Co-LSTO) and SrTiO₃ (STO). The archetypical perovskite STO is widely used as an insulating and diamagnetic substrate for thin film growth. Remarkably, its transport properties can be drastically modified by doping with Nb¹⁴, La¹⁵ or by creating oxygen vacancies, and a transition towards a metallic state occurs for carrier densities as low as $\approx 10^{17}$ cm⁻³ (14,16).

Here, we report the properties of ferromagnetic Co-LSTO thin films grown on STO (001) substrates at low oxygen pressure ($7 \times 10^{-7} \leq P_{O_2} \leq 5 \times 10^{-6}$ mbar). In these conditions, the Co-LSTO films are ferromagnetic with a large intrinsic spin-polarization and the STO substrates are conductive. Both materials have low-temperature resistivities in the m Ω ·cm range and in STO, we find mobilities of up to 10^4 cm²/Vs. Accordingly, Shubnikov-de Haas (SdH) oscillations are observed and their analysis reveal that carriers have long scattering rates of $\tau \approx 10^{-11}$ s, suggesting a spin-diffusion length

exceeding $1\ \mu\text{m}$. We argue that this observation, together with the low carrier density in STO and the large spin-polarization of Co-LSTO, opens the way for the realization of full oxide spin field effect transistors (spin-FET).

II. EXPERIMENTAL

Co-LSTO and LSTO epitaxial thin films were grown on $10\ \text{mm} \times 10\ \text{mm} \times 0.5\ \text{mm}$ STO(001) or LAO(001) ($\text{LAO} : \text{LaAlO}_3$) substrates by pulsed laser deposition (PLD)¹³ from $(\text{La,Sr})\text{Ti}_{1-x}\text{Co}_x\text{O}_3$ targets with $x = 0.02$ and $x = 0$ (see Table I for a summary of the sample description). The La/Sr ratio was about 2:1. The deposition oxygen pressure (P_{O_2}) was varied from 7×10^{-7} mbar to 10^{-4} mbar. For current-perpendicular-to-plane (CPP, Fig. 1(a)) transport measurements in Co-LSTO-based magnetic tunnel junctions (MTJs), a 2.8 nm LAO layer was grown in the same conditions on the Co-LSTO films. The Co-LSTO/LAO bilayers were then covered by a Co/CoO/Au stack, processed into tunnel junctions¹⁷ and measured in standard 4-wire DC configuration. The magnetic properties of thin films were measured with an alternating gradient force magnetometer (AGFM) at room temperature. Current-in-plane (CIP, Fig. 1(b)) magnetotransport measurements were performed on Co-LSTO and LSTO single films in Hall geometry, with an AC set-up (22 Hz) and in magnetic fields up to $B = 16$ teslas and temperatures down to $T = 1.5\text{K}$. Each sample had a pair of current, voltage and Hall contacts, to which $30\ \mu\text{m}$ diameter platinum wires were attached with silver paint. The Hall resistance R_{xy} was measured at fixed temperatures and in field sweepings from maximum negative to maximum positive value, in order to eliminate the possible mixing of magnetoresistive components ($R_{xy} = [R_{xy}(B) - R_{xy}(-B)]/2$). The Hall resistance was linear with the magnetic field for all samples. The mobility was determined as $\mu = L/w(R_{xy}/R_{xx}B)$, where L is the distance between the voltage contacts, w is the width of the specimen and R_{xx} is the CIP-resistance. For the measured samples, L varied between 5 and 6 mm, and $w = 2\ \text{mm}$.

III. MAGNETOMETRY AND CPP MEASUREMENTS: FERROMAGNETISM AND SPIN POLARIZATION OF CO-LSTO

The inset of Fig. 2 shows that Co-LSTO films are ferromagnetic at room temperature, with a maximum saturation magnetization (M_S) of about $5\ \text{emu}/\text{cm}^3$ obtained for films grown at the lowest pressures ($P_{\text{O}_2} \leq 5 \times 10^{-6}$ mbar). We have probed the spin polarization of the Co-LSTO layers by measuring the magnetotransport properties (in CPP geometry) of Co-LSTO/LAO/Co MTJs. The existence of a tunnel magnetoresistance ($\text{TMR} \approx 20\%$, Fig. 2) in these tunnelling experiments demonstrates the spin-polarization of Co-LSTO. The details of these

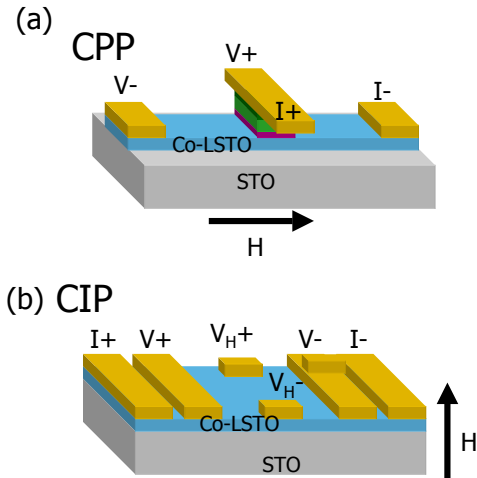


FIG. 1: Geometry of the current-in-plane (CIP) and current-perpendicular-to-plane (CPP) experiments.

experiments with, in particular, the analysis of the peculiar TMR bias dependence and the determination of the spin polarization ($\sim 80\%$) are presented elsewhere¹⁸.

IV. CIP MEASUREMENTS: RESISTANCE AND MOBILITY

We turn now to the CIP measurements of Co-LSTO and LSTO films. The samples grown on STO at low P_{O_2} (samples #1 – #4) show extremely large $\mathfrak{R} = R_{xx}(300\text{K})/R_{xx}(2\text{K})$ ratios ($\sim 700 - 1700$, cf. Fig. 3) and large electronic mobilities at low temperature (up to $\mu \approx 10^4\ \text{cm}^2/\text{Vs}$, cf. Fig. 5). In contrast, a film grown on LAO also at low P_{O_2} (sample #5, cf. Fig. 4) has a $\mathfrak{R} \approx 1.4$ (i. e. about 3 orders of magnitude lower) and poor electronic mobility (around $1\ \text{cm}^2/\text{Vs}$ at $T = 2 - 100\ \text{K}$; cf. Fig. 5). In the same way, a film grown on STO at high $P_{\text{O}_2} = 10^{-4}$ mbar (sample #6, cf. Fig. 4) has also a low ratio $\mathfrak{R} \approx 1.3$ and a mobility $\mu = 5.5\ \text{cm}^2/\text{Vs}$.

Our resistance and mobility data can therefore be summarized as follows. The large values of \mathfrak{R} and μ appear only when Co-LSTO films are grown on STO substrates at low oxygen pressure (samples #1 – #4). Indeed, this conductive behavior, together with a high-

TABLE I: List of samples analyzed in this paper

Sample	Substrate	Co%	$t_{LSTO}(nm)$	$P_{O_2}(mbar)$
#1	STO	0	150	10^{-6}
#2	STO	1.5	150	$8 \cdot 10^{-7}$
#3	STO	1.5	150	10^{-6}
#4	STO	1.5	20	10^{-6}
#5	LAO	1.5	150	$7 \cdot 10^{-7}$
#6	STO	1.5	130	$2 \cdot 10^{-4}$

TABLE II: Transport properties of high-mobility STO substrates

Sample	$\mu_H(1.75\text{ K})$	\Re	$n(10^{18}cm^{-3})$	m_H/m_e	$\rho_{2K}(m\Omega cm)$
#1	2250	695	1.9	0.94	1.5
#2	5950	935	1.1	1.2	1.0
#3	6350	912	1.2	1.2	0.8
#4	10500	1706	1.0	1	0.6

TABLE III: Transport properties of Co-LSTO films

Sample	$\mu_H(1.75\text{ K})$	\Re	$n(10^{18}cm^{-3})$	$\rho_{2K}(m\Omega cm)$
#5	0.9	1.4	9100	0.8
#6	5.5	1.3	1000	1.15

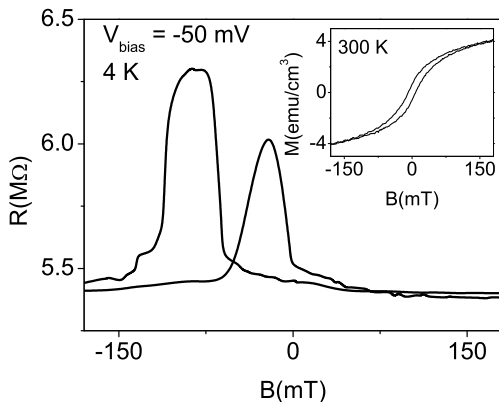


FIG. 2: Field dependence of the resistance of a Co-LSTO/LAO/Co magnetic tunnel junction (size $64\text{ }\mu\text{m}^2$), at 4K and bias-voltage of 50 mV. The inset shows a magnetization hysteresis cycle measured at 300K for a Co-LSTO (1.5%) film grown at 10^{-6} mbar.

mobility, is reminiscent of what was reported for bulk STO single-crystal samples either doped with Nb, treated in reduced atmospheres^{14,16} or etched by accelerated Ar

ions¹⁹. Since the high \Re and μ are observed for the films grown in the most reducing conditions (i.e., promoting the creation of oxygen vacancies), the high-mobility and low resistance state come most likely from the STO substrate. On the other hand, LAO or high- P_{O_2} STO are insulators, and the measured transport properties of samples #5 and #6 are probably intrinsic of Co-LSTO. Thus, in our interpretation, the transport properties displayed in Table II (samples #1 – #4) refer to the STO substrate, whereas Table III (samples #5 – #6) corresponds to the electronic properties of Co-LSTO.

We note that it is remarkable that the conditions necessary to grow the DMOS with a large spin-polarization generate this high-mobility state in the STO. The thickness over which the high-mobility state is created in STO is discussed later.

V. CIP MEASUREMENTS: SDH IN HIGH-MOBILITY STO COVERED BY CO-LSTO OR LSTO

Magnetic field and temperature dependence of the CIP resistance R_{xx} for sample #2 is shown in Fig. 6. The magnetic field H was applied perpendicularly to the sample plane. A large positive perpendicular magnetoresistance (PMR = $(R_{xx}(H) - R_{xx}(0))/R_{xx}(0)$) is observed, show-

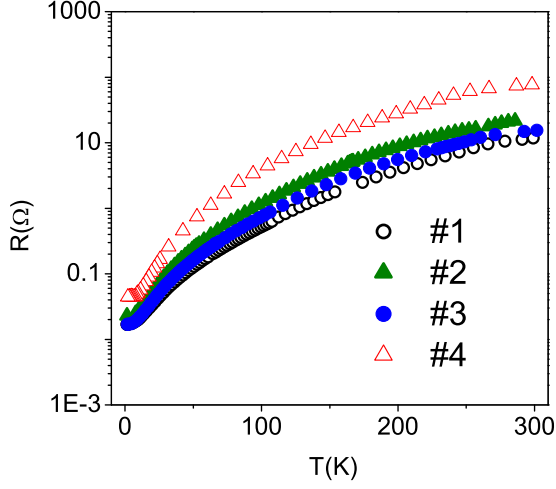


FIG. 3: Temperature dependence of the raw resistance of samples #1 – #4.

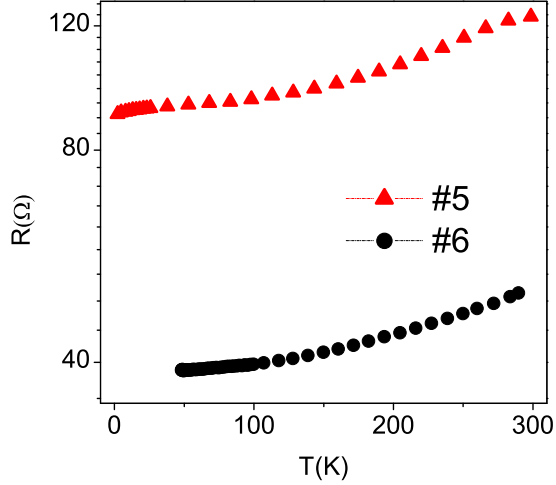


FIG. 4: Temperature dependence of the raw resistance of samples #5 and #6.

ing oscillations (at $T \leq 4$ K and $\mu_H \geq 6$ T) that are due to the Shubnikov-de Haas (SdH) effect. We emphasize that we have observed SdH oscillations in all other high-mobility samples. Oscillations with the same period are also observed when the field is applied parallel to the sample plane in the longitudinal configuration (not shown). Such observation evidences that the high-mobility region is 3D-like and is not an interface effect. Quantum transport effects like SdH oscillations are usu-

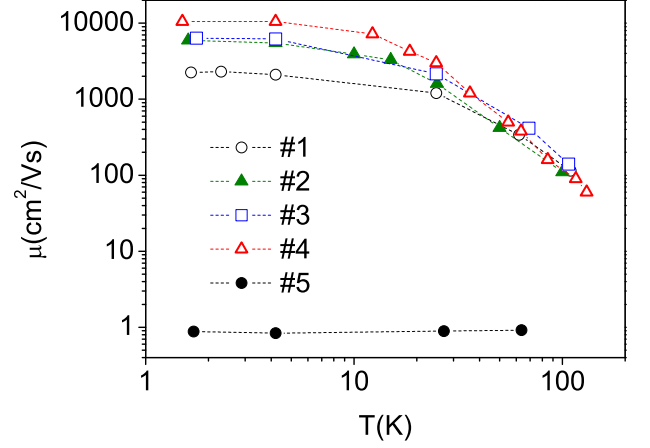


FIG. 5: The temperature dependence of the electronic mobilities (μ_H) for samples grown on STO at $P_{O_2} < 10^{-6}$ mbar and on LAO ($P_{O_2} < 10^{-6}$ mbar).

ally observed in systems with high mobilities. This is the case of semi-metals like Bi²⁰ or semiconductors like GaAs²¹, but SdH oscillations have been very seldom observed in oxide materials^{22,23,24}.

In order to isolate the SdH oscillations, first a background positive magnetoresistance R_{bkgnd} was determined by fitting the experimental data R_{xx} to a low-order polynomial (cf. inset of Fig. 6). The oscillating part ΔR_{SdH} of the magnetoresistance was then obtained as $\Delta R_{SdH} = R_{xx} - R_{bkgnd}$. Fig. 7 shows that ΔR_{SdH} scales with mobility μ in the same way as does the perpendicular magnetoresistance PMR. The origin of the large values of the PMR is presumably related to the perturbation of the electronic orbitals by the applied field and, thus, they are more significant when the mean free path, i. e. the mobility, is larger. Our results indicate that both SdH amplitudes and PMR originate from similar physical mechanisms.

Fig. 8 presents the oscillations of ΔR_{SdH} as a function of $1/B$ and temperature. We analyzed these SdH oscillations in our samples using the conventional Lifshitz-Kosevich expression²⁵. The amplitude of the oscillation is given as:

$$\Delta R_{SdH} \propto B^{1/2} R_T R_D R_S \sin \left[2\pi \left(\frac{F}{B} - \frac{1}{2} \right) \pm \frac{\pi}{4} \right] \quad (1)$$

where ΔR_{SdH} is the amplitude of the SdH-oscillating part of the resistance, and $F = \hbar A / 2\pi e$ (A is the extremal orbit area in k-space perpendicular to the applied field) is expressed in teslas. The oscillation amplitude is damped due to the smearing of the Fermi surface orbit by temperature (R_T), scattering (R_D) and spin-splitting effects (R_S):

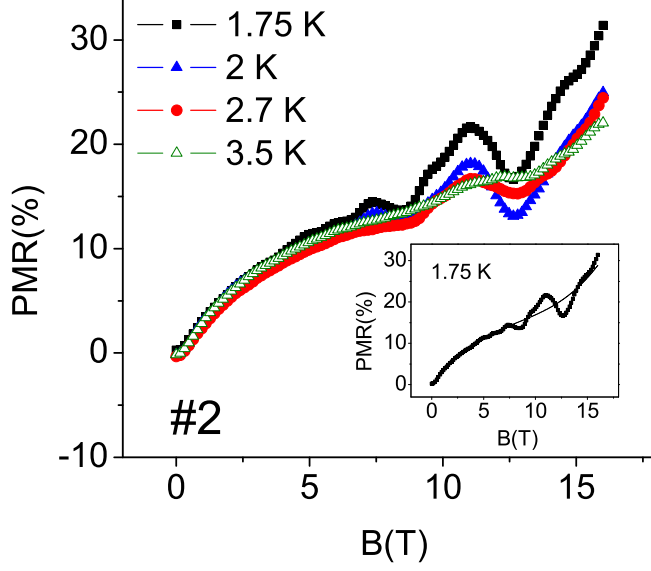


FIG. 6: Magnetic field dependence of resistance of sample #2 at different temperatures, showing SdH oscillations. The inset shows the background resistance R_{bkgnd} (solid line) obtained by fitting a cubic polynomial.

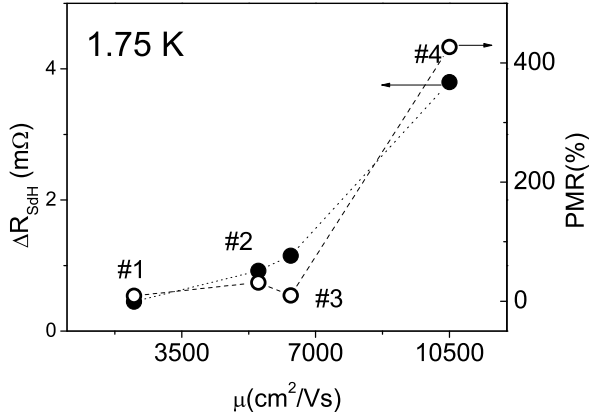


FIG. 7: The mobility dependence of the SdH-oscillation amplitude ΔR_{SdH} and the PMR (for $B = 16$ T) for samples #1 – #4.

$$R_T = \frac{\alpha(m_H/m_e)T/B}{\sinh(\alpha(m_H/m_e)T/B)} \quad (2)$$

with $\alpha = (2\pi^2 k_B m_e)/e\hbar = 14.69$ (TK⁻¹);

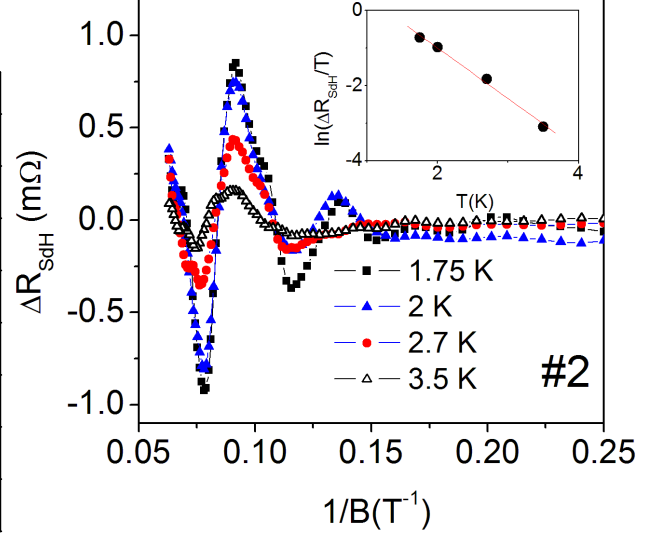


FIG. 8: SdH-oscillation amplitudes ΔR_{SdH} vs. $1/B$ for sample #2 at different temperatures. The inset shows the extraction of the effective mass from the $\ln \Delta R_{SdH}/T$ vs. T plot.

$$R_D = \exp\left(\frac{-\alpha(m_H/m_e)T_D}{B}\right) \quad (3)$$

where m_H is the effective mass, $T_D = \hbar/(2\pi k_B \tau)$ is the Dingle temperature and τ is the scattering rate;

$$R_S = \cos[(\pi/2)g_{eff}(m_H(\theta)/m_e)] \quad (4)$$

where g_{eff} is the effective Landé factor.

A Fast Fourier Transform (FFT) method has been used to obtain the power spectra of the measured resistance values. This analysis indicates a primary frequency of $F \approx 24 - 35$ T, depending on sample (Fig. 9). The data also suggest the presence of higher-frequency components; however, their amplitude is much lower, and therefore they will be neglected in the following discussion. From the frequency F we can infer the cross-sectional area A of the closed electronic orbits contributing to the SdH oscillations. Experimental data support a conduction band of STO consisting of ellipsoids of revolution having the long axis along the $\langle 100 \rangle$ crystalline axes, and minima at the Γ -points^{16,26,27}. Taking into account this k-space geometry and the value of k_F , we can estimate the carrier density as $n \approx 1.0 \times 10^{18} - 1.9 \times 10^{18}$ cm⁻³ (see Table II and section VIII). We observe that the mobility increases with decreasing n (cf. inset of Fig. 9), in agreement with previous reported works¹⁴. This may be explained by assuming that oxygen vacancies act as carrier donors, being simultaneously scattering centers.

In comparison, the carrier density of sample #5 (Co-LSTO on LAO) deduced from Hall experiments is $n \approx$

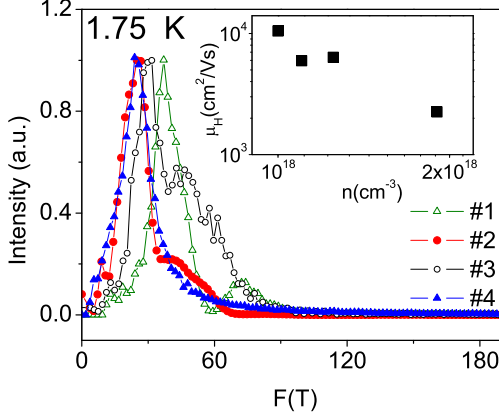


FIG. 9: Power Spectrum Intensity of SdH oscillations at $T = 1.75$ K of samples #1 – #4. The inset shows the evolution of the Hall mobility with the carrier density (extracted from the frequency of the SdH oscillations).

$9 \times 10^{21} \text{ cm}^{-3}$. We recall that in this case the Hall experiments allow the extraction of the electronic properties of the film, since the substrate is an insulator. The measured carrier density is consistent with about 0.6 carrier per formula unit, which is in a good agreement with what is expected from the film composition, assuming the presence of some oxygen vacancies.

For the high-mobility samples (#1 – #4), the effective mass (m_H) of the carriers in STO was estimated by analyzing the temperature dependence of the SdH oscillations amplitude and plotting $\ln(\Delta R_{SdH}/T)$ vs. temperature. This expression is accurate within an error $< 2\%$ and can be deduced from Eq. (1), assuming that $T/B \geq 0.14/(m_H/m_e)$ (KT^{-1}). We have checked this condition after the extraction of m_H . Our analysis yields the values of m_H between $0.94 - 1.2m_e$ (cf. Table II). The Dingle temperature T_D was obtained from the slope of the plot of $\ln(\Delta R_{SdH} B^{1/2} \sinh(\alpha(m_H/m_e)T/B))$ versus $1/B$ at $T = 1.75$ K. Due to the limited number of oscillations in the explored range of field values, this analysis turned out to be quite difficult. Nevertheless, values of $T_D = 0.3 - 1$ K were obtained, corresponding to scattering rates $\tau_D = 4 - 12 \times 10^{-12}$ s. The values of τ_D correspond to the scattering rates of the closed electronic orbits around the extremal cross sections of the Fermi surface. Due to the cubic symmetry of STO, we can estimate the scattering rate $\tau = \frac{\mu m_H}{e}$ at low temperature, assuming that the effective mass is isotropic and equal to m_H . Using the values of μ and m_H (table II) we get $\tau = 1.5 - 6 \times 10^{-12}$, in good agreement with the values of τ_D .

Knowing the carrier densities and mobilities, we can calculate the resistivity through $\rho_{xx} = 1/(ne\mu)$. We find increasing values in the range $\rho_{xx} = 0.6 - 1.5 \text{ m}\Omega \text{ cm}$, for decreasing mobilities within the range $2250 - 10500$

cm^2/Vs (see Table II). These values of ρ_{xx} are consistent with those from the literature, for similar mobility values¹⁴.

The values of ρ_{xx} and n allow us to estimate the order of magnitude of the thickness t_{STO} of the high mobility region inside the STO. From $\rho_{xx} = (wt_{\text{STO}})R_{xx}/L$, with $L \approx 5 - 6 \text{ mm}$ and $w \approx 2 \text{ mm}$, we infer $t_{\text{STO}} \approx 300 - 900 \mu\text{m}$. We can also estimate t_{STO} from the measured Hall constant $R_H = 1/ne = R_{xy}t_{\text{STO}}/B$, and assuming the values of the carrier densities extracted from the SdH analysis (Table II) we find again $t_{\text{STO}} \approx 300 - 900 \mu\text{m}$. In other words, the high mobility system is not an interfacial interface effect, but it is extended to a sizable part of the STO substrate. This is also supported by the observation of SdH oscillations when the magnetic field is applied in the film plane in the longitudinal configuration (see section V). An additional support for this conclusion comes from the estimation of the spread of the oxygen vacancy diffusion in STO, by using the diffusion constants determined experimentally from optical experiments²⁸. Even in the less favorable case (considering trapping effects due to impurities inside the STO, and at pressures $P_{O_2} \approx 10^{-2} \text{ mbar}$, i. e. around four orders of magnitude higher than our growth conditions), the determined diffusion constants were $D \approx 10^{-4} \text{ cm}^2/\text{s}$ at $T \approx 700^\circ\text{C}$; with this value, the diffusion of O-vacancies during the deposition time $t_{\text{dep}} \approx 10^2 - 10^3 \text{ s}$ can be estimated to be $l_{\text{ovac}} \approx (D \times t_{\text{dep}})^{1/2} \approx 1 \text{ mm}$. Thus, the oxygen vacancies can diffuse across the STO substrate, which is consistent with the $t_{\text{STO}} \approx 300 - 900 \mu\text{m}$ we found from transport data.

VI. PERSPECTIVES

The resistivity of the Co-LSTO films can be calculated from the resistance of the LAO//Co-LSTO and high- P_{O_2} STO//Co-LSTO samples and the Co-LSTO film thickness. This yields $0.9 \text{ m}\Omega \cdot \text{cm}$ and $1.15 \text{ m}\Omega \cdot \text{cm}$ at low temperature, respectively, see Table III. Thus, the low-temperature resistivities of the Co-LSTO films and the oxygen-deficient STO substrates are in the $\text{m}\Omega \cdot \text{cm}$ range. Due to the high mobility of the latter, it is tempting to consider the possibility of spin-injection from Co-LSTO into STO, as in the Co/Cu case. More precisely, in this case the spin-polarization of the injected current is given by⁵

$$P = \beta/(1 + r_N/r_F) = \beta/[1 + (\rho_N l_{sf}^N/\rho_F l_{sf}^F)] \quad (5)$$

with β being related to the spin-up resistivity ρ_\uparrow and spin-down resistivity ρ_\downarrow channels in the ferromagnet by $\beta = (\rho_\uparrow - \rho_\downarrow)/(\rho_\uparrow + \rho_\downarrow)$. ρ_F , ρ_N and l_{sf}^F , l_{sf}^N are the resistivities and the spin diffusion length in the ferromagnet and the non-magnetic material, respectively. In the present case, we know $\rho_N/\rho_F \approx 1$ and β should be close to -1 as the spin-polarization of Co-LSTO is $\sim 80\%$ ¹⁸. In conventional metals, l_{sf} is usually much longer

than the mean free path λ . Here $\lambda_{STO} \geq 100$ nm and $\lambda_{Co-LSTO} \approx 1$ nm but the spin diffusion lengths are unknown for virtually all oxide materials.

Since oxygen-deficient STO thin films with mobilities and resistivities comparable to those reported for single crystals have already been fabricated^{29,30}, Co-LSTO/STO superlattices could exhibit a significant CPP GMR and systematic GMR studies should allow measuring l_{sf} in both materials.

It must be pointed out that the efficient spin-injection from Co-LSTO into STO may be limited to the lowest temperatures due to the steep increase of resistivity of STO (cf. Fig. 3). However, if the r_N/r_F ratio turns out to be too large to allow an efficient spin-injection, the latter could be increased by inserting for instance, an ultrathin tunnel barrier of LAO⁵. Our TMR measurements indeed demonstrate that in the low oxygen pressure conditions required to obtain ferromagnetic Co-LSTO and high-mobility STO, LAO retains its insulating properties.

Finally, we would like to mention that several groups have fabricated FETs using STO as the channel material, with gains reaching 100 at room temperature³¹. Remarkably, the field effect proves efficient for a wide range of carrier density, from the undoped³¹ to the metallic state ($n \approx 10^{18}$ cm⁻³)³⁰ and even in the low-temperature superconducting phase³². If the field effect can modify the spin-diffusion length (in addition to the carrier density), or enables the tuning of spin-flip mechanisms (in analogy to the principle of the Datta and Das transistor³³), full oxide spin-FET using STO channels and Co-LSTO as spin injector and detector could be built in the near future.

VII. CONCLUSION

In conclusion, we have demonstrated the feasibility of growing a full oxide structure combining a highly spin polarized diluted magnetic system Co-LSTO and high-mobility (up to $\approx 10^4$ cm²/Vs) STO, by using low oxygen pressure growth conditions. At low temperatures and high magnetic fields, we have observed Shubnikov-de Haas oscillations in the resistance of the STO. Careful analysis of this behavior for several samples has allowed us to extract valuable information on the electronic properties of the high-mobility STO. Besides the very large mobility, we have found that the metallic state of STO occurs for carriers densities as low as $\sim 10^{18}$ cm⁻³, with large scattering rates up to $\approx 10^{-11}$ s. The combined properties of the two materials -i. e. the large spin-polarization of Co-LSTO and the long mean free path

of STO - makes them interesting to realize spin-injection devices like spin FET, the low carrier density of STO enabling external control by gate voltage. Several studies have recently demonstrated the potential of Ti perovskites for oxide electronics^{34,35,36}. We are convinced that our findings extend this potential to oxide spintronics.

VIII. ANNEX: ESTIMATION OF THE CARRIER DENSITY FROM SDH OSCILLATIONS

The Fermi surface of STO is composed of three ellipsoids of revolution centered at Γ -points with the long axis $k_{F,max}$ along $\langle 100 \rangle$ crystallographic axes and the short $k_{F,min}$ axes transverse to them^{16,26,27}. The ratio between the longitudinal (m_l) and transverse (m_t) masses have been determined experimentally as $m_l/m_t \approx 4$ ^{16,26}. Recalling that $\partial^2 E(\mathbf{k})/\partial \mathbf{k}^2 \propto 1/m$, we can infer that $k_{F,max}/k_{F,min} \approx 4$.

Let us assume that a field H_z is applied along the $[001]$ direction. Then the extremal electronic closed orbits corresponding to the 2 spheroids directed along x- and y-axis are ellipsoidal with cross sections equal to $\pi \cdot k_{F,min} \cdot k_{F,max}$, whereas the cross sections of the ellipsoid along the z-direction is circular with an area $\pi \cdot k_{F,min}^2$. In addition, since $k_{F,max}/k_{F,min} \approx 4$ there are about 4 more electrons around the ellipsoidal closed orbits than those orbiting the circular orbits. Taking into account these facts, we assume that the main frequency peak of the ΔR_{SDH} oscillations comes from electrons orbiting the ellipsoidal cross sections, and, thus, $A = \pi \cdot k_{F,min} \cdot k_{F,max}$. As the total volume in the k-space occupied by the 3 ellipsoids is $V_{\mathbf{k}} = 3 \times \frac{4\pi}{3} k_{F,min}^2 k_{F,max}$, we can estimate the carrier concentration as $n = 3 \times \frac{k_{F,min}^2 k_{F,max}}{3\pi^2}$.

Acknowledgments

We are grateful to P. Berthet, C. Pascanut and N. Dragoe for providing the Co-LSTO target. G. Herranz acknowledges financial support from Ministère de l'Education Nationale, de l'Enseignement Supérieur et de la Recherche (France) and R. Ranchal thanks Universidad Complutense de Madrid and the Spanish Project MAT 2001-3554-CO2 for partially supporting her stay at UMR137, CNRS-Thales at Orsay, France. The financial support from the PAI-France-Croatia COGITO program n° 82/240083 is also acknowledged.

* Electronic address: gervasi.herranz@thalesgroup.com

¹ M.N. Baibich, J.M. Broto, A. Fert, F. Nguyen Van Dau, F. Petroff, P. Eitenne, G. Creuzet, A. Friederich, and

- J. Chazelas, Phys. Rev. Lett. **61**, 2472 (1995).
- ² J. S. Moodera, L. R. Kinder, T. M. Wong, and R. Meservey, Phys. Rev. Lett. **74**, 3273 (1995).
- ³ I. Žutić, J. Fabian, and S. Das Sarma, Rev. Mod. Phys. **76**, 323 (2004).
- ⁴ G. Schmidt, D. Ferrand, L.W. Molekamp, A.T. Philip, and B.J. van Wees, Phys. Rev. B **62**, R4790 (2000).
- ⁵ A. Fert and H. Jaffrès, Phys. Rev. B **64**, 184420 (2001).
- ⁶ E.I. Rashba, Phys. Rev. B **62**, R16267 (2000).
- ⁷ R. Fiederling, M. Kleim, G. Reuscher, W. Ossau, G. Schmidt, A. Waag, and L.W. Molekamp, Nature (London) **402**, 787 (1999).
- ⁸ D. K. Young, E. Johnston-Halperin, D.D. Awschalom, Y. Ohno, and H. Ohno, Appl. Phys. Lett. **80**, 1598 (2002).
- ⁹ A.H. MacDonald, P. Schiffer, and N. Samarth, Nat. Mater. **4**, 195 (2005).
- ¹⁰ Y. Matsumoto, M. Murukami, T. Shono, T. Hasegawa, T. Fukumura, M. Kawasaki, P. Ahmet, T. Chikyow, S. Koshihara, and H. Koinuma, Science **192**, 854 (2001).
- ¹¹ J.M.D. Coey, M. Venkatesan, and C.B. Fitzgerald, Nat. Mater. **4**, 173 (2005).
- ¹² Y.G. Zhao, S.R. Shinde, S.B. Ogale, J. Higgins, R.J. Choudhary, V.N. Kulkarni, R.L. Greene, T. Venkatesan, S.E. Lofland, C. Lanci, et al., Appl. Phys. Lett. **83**, 2199 (2003).
- ¹³ R. Ranchal, M. Bibes, A. Barthélemy, K. Bouzehouane, S. Guyard, E. Jacquet, J.-P. Contour, C. Pascanut, P. Berthet, and N. Dragoe, J. Appl. Phys. **98**, 013514 (2005).
- ¹⁴ O.N. Tufte and P.W. Chapman, Phys. Rev. **155**, 796 (1967).
- ¹⁵ Y. Tokura, Y. Taguchi, Y. Okada, Y. Fujishima, T. Arima, K. Kumagai, and Y. Iye, Phys. Rev. Lett. **470**, 2126 (1993).
- ¹⁶ H.P.R. Frederikse, W.R. Thurber, and W.R. Hosler, Phys. Rev. **134**, A442 (1964).
- ¹⁷ M. Bowen, M. Bibes, A. Barthélémy, J.-P. Contour, A. Anane, Y. Lemaître, and A. Fert, Appl. Phys. Lett. **82**, 233 (2003).
- ¹⁸ G. Herranz, R. Ranchal, M. Bibes, H. Jaffrès, E. Jacquet, J.-L. Maurice, K. Bouzehouane, F. Wyczisk, E. Tafr, M. Basletic, et al. (2005), unpublished, available at <http://arXiv.org/cond-mat/0508289>.
- ¹⁹ D.W. Reagor and V.Y. Butko, Nat. Mater. **4**, 593 (2005).
- ²⁰ L.S. Lerner, Phys. Rev. **130**, 605 (1963).
- ²¹ B.M. Vul, E.I. Zavaritskaya, N.V. Kotelnikova, and I.D. Voronova, Sov. Phys. Semicond. **10**, 751 (1976).
- ²² H.P.R. Frederikse, W.R. Hosler, W.R. Thurber, J. Babiskin, and P.G. Siebenmann, Phys. Rev. **158**, 775 (1967).
- ²³ A.P. Mackenzie, J.W. Reiner, A.W. Tyler, L.M. Galvin, S.R. Julian, M.R. Beasley, T.H. Geballe, and A. Kapitulnik, Phys. Rev. B **58**, R13318 (1998).
- ²⁴ G. Cao, L. Balicas, Y. Xin, J.E. Crow, and C.S. Nelson, Phys. Rev. B **67**, 184405 (2003).
- ²⁵ D. Schoenberg, *Magnetic Oscillations in Metals* (Cambridge University Press, Cambridge, UK, 1984).
- ²⁶ A. H. Kahn and A. J. Leyendecker, Phys. Rev. **135**, A1321 (1964).
- ²⁷ L.F. Mattheiss, Phys. Rev. B **6**, 4718 (1972).
- ²⁸ I. Denk, F. Noll, and J. Maier, J. Am. Ceram. Soc. **80**, 279 (1997).
- ²⁹ A. Leitner, C.T. Rodgers, and J.C. Price, Appl. Phys. Lett. **72**, 3065 (1998).
- ³⁰ I. Pallecchi, G. Grassano, D. Marré, L. Pellegrino, M. Putti, and A.S. Siri, Appl. Phys. Lett. **78**, 2244 (2001).
- ³¹ K. Ueno, I.H. Inoue, H. Akoh, M. Kawasaki, Y. Tokura, and H. Takagi, Appl. Phys. Lett. **83**, 1755 (2003).
- ³² K.S. Takahashi, D. Matthey, D. Jaccard, J.-M. Triscone, K. Shibuya, T. Ohnishi, and M. Lippmaa, Appl. Phys. Lett. **84**, 1722 (2004).
- ³³ D. Datta and B. Das, Appl. Phys. Lett. **56**, 665 (1990).
- ³⁴ A. Ohtomo, D.A. Muller, J.L. Grazul, and H.Y. Hwang, Nature **419**, 378 (2002).
- ³⁵ A. Ohtomo and H.Y. Hwang, Nature **427**, 423 (2004).
- ³⁶ S. Okamoto and A.J. Millis, Nature **428**, 630 (2004).